coatings

MDPI

Article

Multifunctional Janus Coatings for Synergistic Photothermal and Radiative Regulation in Adaptive Textiles

Qingman Liu [1], Hanqi Li [1], Hao Wang [1], Ziyi Zang [1], Wanqi Cui [1], Yongli Yu [1], Li Li [2], Xiaohu Wu [3,4,5,*] and Xiansheng Zhang [1,*]

[1] Shandong Key Laboratory of Medical and Health Textile Materials, College of Textiles and Clothing, Qingdao University, Qingdao 266071, China
[2] Shaanxi Yuanfeng Prosafe Co., Ltd., Xi'an 710025, China
[3] School of Integrated Circuits, Hubei University, Wuhan 430062, China
[4] Yangtze Laboratory, Wuhan 430205, China
[5] Thermal Science Research Center, Shandong Institute of Advanced Technology, Jinan 250100, China
* Correspondence: wuxiaohu@pku.org.cn (X.W.); xshzhang@qdu.edu.cn (X.Z.)

Highlights

What are the main findings?

- A Janus textile with phase-change/thermochromic front and MXene back was fabricated.
- SiO_2-encapsulated 1-tetradecanol microcapsules show high latent heat (121 J/g) and thermal stability.
- The textile reversibly switches from black to white at approximately 29 °C, suppressing sunlight-induced overheating.
- MXene layer provides 40–65 °C Joule heating at 3–5 V and 20 dB EMI shielding (absorption-dominated).
- The textile exhibits hydrophobicity with a mean static water contact angle of 130.2° and self-cleaning ability.

What are the implications of the main findings?

- Enables all-season personal thermal management without continuous energy input.
- Achieves synergy between passive radiative/phase-change regulation and active electrothermal heating.
- Offers a new strategy for smart protective clothing and multifunctional field tents.
- Demonstrates potential in anti-counterfeiting, information encryption, and non-contact display.
- Provides a scalable fabrication route (sol-gel, screen printing, spray coating) for Janus smart textiles.

Abstract

The escalating energy crisis and global warming drive the demand for all-season self-regulating functional textiles. This study presents a Janus smart textile that combines phase change energy storage with active and passive heating modes, electromagnetic interference shielding, and self-cleaning capabilities. The front surface incorporates phase change temperature regulation and thermochromic properties, while the back surface is spray-coated with a transition metal carbide to establish a continuous conductive network. In the low-temperature state, the black surface enhances solar absorption for efficient heating; as the temperature rises, the surface turns white to increase solar reflection and suppress overheating. This mechanism, combined with phase change energy storage, enables the textile to mitigate environmental temperature fluctuations. The MXene layer on the back

Check for updates

Academic Editor: Jiri Militky

Received: 11 April 2026
Revised: 6 May 2026
Accepted: 8 May 2026
Published: 11 May 2026

Copyright: © 2026 by the authors. Licensee MDPI, Basel, Switzerland. This article is an open access article distributed under the terms and conditions of the Creative Commons Attribution (CC BY) license.

provides efficient Joule heating and cycling stability under driving voltages of 3 to 5 volts, along with electromagnetic interference shielding dominated by absorption loss. The front hybrid coating further imparts hydrophobic self-cleaning performance. This study offers a strategy for synergistic active and passive thermal management, demonstrating application potential in intelligent outdoor gear and specialized protective outer layers.

Keywords: phase change microcapsule; thermochromic; synergistic thermal management; MXene; smart textile

1. Introduction

The human body, acting as a dynamic thermodynamic system, relies heavily on the thermal exchange balance among the skin and clothing as well as the surrounding environment [1–4]. However, conventional textiles are frequently restricted by their static heat conduction characteristics, making it difficult to cope with intense environmental fluctuations or extreme conditions such as severe cold and high temperatures [5–7]. The common approach of altering environmental temperatures through energy consumption cannot fundamentally address the high efficiency and real time requirements for human thermal comfort. Consequently, the development of efficient and sustainable self-adaptive personal thermal management systems has become an urgent necessity in the fields of materials science and energy [8]. Endowing textiles with the capability to actively perceive the environment and spontaneously regulate heat flow, namely achieving a paradigm shift from static barriers to dynamic responses, holds profound scientific significance and practical value [9–14].

In the realm of passive thermal management, the coupling of self-adaptive radiative regulation and phase-change energy storage has demonstrated tremendous potential [15–18]. Thermochromic materials perceive ambient temperature and undergo reversible molecular structural transitions. This enables a dynamic shift from high absorption at low temperatures to high reflection at high temperatures across the visible and near-infrared spectra [19–24]. Reliance on solitary radiative temperature control is frequently accompanied by temperature oscillations resulting from response delays, thereby posing significant challenges in maintaining a constant microclimate [25]. In the field of human thermal comfort, phase change materials can withstand intense environmental temperature fluctuations through spontaneous heat absorption and release, thereby maintaining the stability of the microclimate on the skin surface. Zhu et al. developed a dual mode photonic textile by integrating phase change materials with thermochromic materials as a surface coating. This textile possesses the dual capabilities of high temperature radiative cooling and low temperature solar heating, which facilitates effective thermal management under significant ambient temperature fluctuations [26]. As a type of bio-based phase change material characterized by low cost and industrial prevalence as well as excellent chemical stability, 1-tetradecanol serves as an effective thermal buffer. Owing to its melting point near 38–40 °C within the human thermal comfort range and its ability to reversibly absorb and release substantial latent heat during solid–liquid phase transitions, 1-tetradecanol serves as an effective phase change material for textile-based thermal management [27]. Alkan et al. employed Pickering emulsion technology to produce microencapsulated phase change materials consisting of a poly methyl methacrylate shell and a 1-tetradecanol core [28]. Upon being incorporated into cement mortar, these materials demonstrated significant potential to enhance thermal comfort within buildings and reduce heating fuel consumption, consequently leading to a reduction in carbon emissions. In practical production and application, the persistent leakage issue of phase-change materials has

significantly restricted their large-scale deployment. Encapsulating these materials within SiO_2 inorganic shells, which are characterized by high mechanical strength, chemical stability, and exceptional optical transparency, has been proven as an effective strategy to bolster the thermal stability and service life of phase-change materials [29–33]. The intricate nature of outdoor environments presents a rigorous test for the weather endurance of intelligent textiles. By incorporating a low surface energy polydimethylsiloxane (PDMS) matrix to establish a hydrophobic self-cleaning surface, the interference of external liquid contaminants on the optical regulation performance is effectively mitigated, while the structural integrity of the internal functional components is ensured throughout long term service [34–36]. Furthermore, with the ubiquity of electronic devices, the human body is continuously exposed to electromagnetic waves. Although such exposure may not immediately impact health, the integration of electromagnetic interference (EMI) shielding functionality into daily apparel has emerged as a prominent focus in the development of multifunctional textiles [37,38]. The development of multifunctional smart textiles that integrate adaptive temperature regulation with EMI shielding is essential for harmonizing personal comfort with a high-quality lifestyle. As a novel class of two-dimensional transition metal carbides, MXene provides an ideal material platform for high performance active heaters and electromagnetic interference shielding devices owing to its exceptional metallic conductivity and efficient photothermal and electrothermal conversion capacities alongside a unique multi layered stacking architecture [39–43]. These attributes facilitate the integration of active thermal modulation and electromagnetic protection with the foundational passive regulation system to achieve advanced multi-functional integration [44]. By leveraging the distinct functionalities of the thermochromic layer and the electromagnetic interference shielding layer, the developed textile holds promising prospects in various fields such as confidentiality [45], dynamic camouflage [46], and infrared stealth [47]. Shao et al. developed an electroactive hydrogel ink by combining transition metal carbides with a polyvinylidene fluoride polymer matrix which was subsequently impregnated onto carbon fibers to construct fiber composites featuring a core shell architecture [48]. This approach significantly enhanced the electrothermal and magnetic properties of the material while achieving notable progress in electromagnetic interference protection and the reduction of mid infrared emissivity.

In summary, inspired by the concept of asymmetric functional integration in the biological world, this study designed and fabricated an all-weather intelligent temperature regulating textile with a Janus architecture (FC-TMs). This textile ingeniously synergizes active electrothermal heating with passive radiative regulation and energy storage. The front side, serving as the passive layer, was functionalized via a screen-printing process where self-synthesized SiO_2 encapsulated phase change material microcapsules (TMs) and commercial thermochromic components were uniformly embedded within a PDMS system. By enabling spontaneous optical switching and latent heat buffering, this layer achieves precise modulation of environmental radiative energy. Simultaneously, the back side, acting as the active layer, incorporates a continuous MXene conductive network constructed through a spray coating technique. This network leverages efficient Joule heating effects to provide on demand thermal compensation while endowing the textile with electromagnetic interference shielding effectiveness (Figure 1a). This dual sided heterogeneous design enables a synergistic transition from passive thermal buffering to active thermal compensation. This study achieves precise regulation of the human microclimate across a broad temperature range while maintaining a balance between electromagnetic protection and environmental robustness. It thus provides an effective design strategy for next-generation high-performance outdoor protective outer layers and multifunctional all-weather field tents.

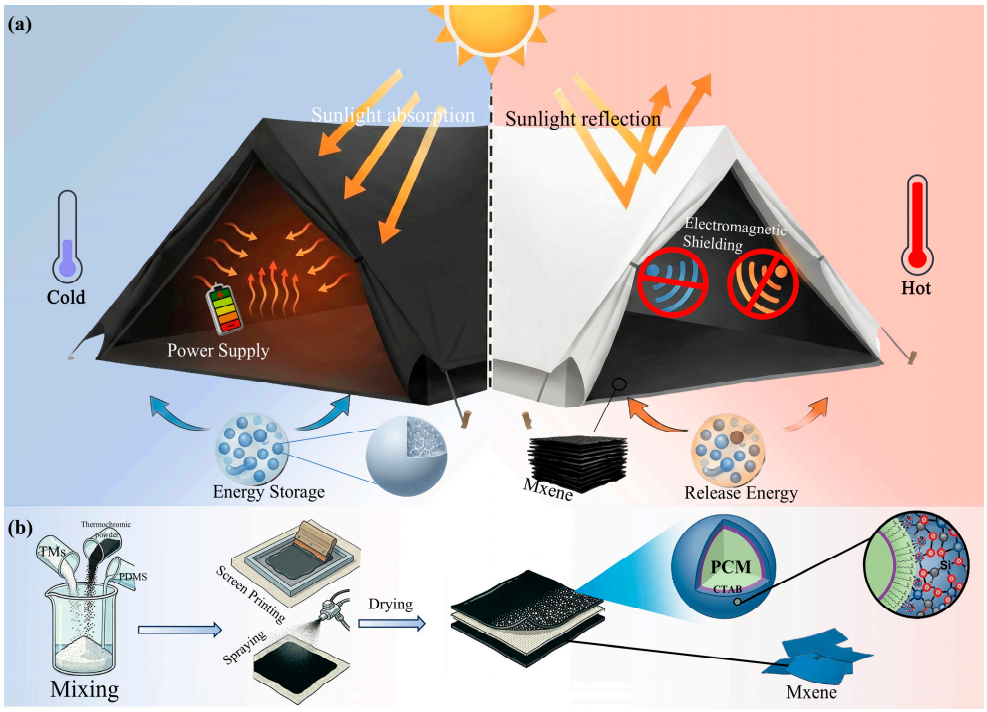


Figure 1. (**a**) Phase change energy storage and release along with photothermal regulation via color transition and electrothermal heating as well as electromagnetic interference shielding of the TMs; (**b**) Schematic illustration of the FC-TMs composite coating on fabric.

2. Experimental

2.1. Materials

1-tetradecanol ($C_{14}H_{30}O$, phase change material), tetraethyl orthosilicate (TEOS, silica source) and hexadecyltrimethylammonium bromide (CTAB, emulsifier) were purchased from Aladdin Bio Chem Technology Co., Ltd. (Shanghai, China). Commercial black thermochromic micro-capsules (color transition temperature 29 °C) were obtained from Shenzhen Color Technology Co., Ltd. MXene nanosheet dispersion ($Ti_3C_2T_x$) was purchased from Jinan Sanchuan New Materials Technology Co., Ltd. (Jinan, China). Polydimethylsiloxane (PDMS, Sylgard 184) and its curing agent were purchased from Dow Chemical Company (Midland, MI, USA). General reagents including anhydrous ethanol, concentrated hydrochloric acid and concentrated ammonia were of analytical grade (Shanghai Aladdin, Shanghai, China). Deionized water was used as the experimental water. The substrate fabric was commercial pure cotton plain weave fabric.

2.2. Preparation of SiO_2 Encapsulated 1-Tetradecanol Microcapsules

Phase change TMs with a core shell structure were prepared via a sol gel method. First, the core material emulsion was prepared by melting 15 g 1-tetradecanol in a 50 °C water bath and adding it into 450 mL aqueous solution containing 1.5 g CTAB. The mixture was emulsified using a high-speed shear emulsifier (8000 rpm) for 20 min to obtain a stable oil in water emulsion for later use. Then, the silica sol precursor was prepared by mixing 30 g TEOS with 30 g anhydrous ethanol, followed by the dropwise addition of 1.0 mol L^{-1} hydrochloric acid under stirring to adjust the pH to 2.0. The reaction was conducted at 50 °C for 2 h to obtain a transparent silica sol. At 45 °C, the silica sol was dripped into the core material emulsion at a constant rate and reacted for 1 h. Subsequently, ammonia was slowly added at a rate of 2.0 mL h^{-1} using a syringe pump to adjust the system pH to 8.5 to 9.0 to trigger the polycondensation of SiO_2. After reacting for 24 h and subsequent

aging, the product was filtered and washed alternately with deionized water and ethanol. Finally, the white powder of TMs was obtained after vacuum drying at 40 °C.

2.3. Preparation of Multifunctional Janus Structured Textiles

The front surface layer, serving as the passive temperature regulation layer, was fabricated by mixing self-synthesized phase change TMs at a weight percentage of 45 wt% and commercial thermochromic microcapsules at a weight percentage of 5 wt% with a PDMS matrix according to a specific proportion. The mixture was processed through ultrasonic degassing to ensure the complete removal of air bubbles. Subsequently, the resulting slurry was uniformly applied to the upper surface of the cotton fabric via screen printing technology. The fabric was then leveled at room temperature for 15 min and cured at 80 °C for 2 h to yield a composite coating characterized by self-adaptive temperature control and hydrophobic properties. Simultaneously, the back surface layer, which acts as the active electrothermal and EMI shielding layer, was prepared by uniformly spraying MXene dispersion onto the reverse side of the fabric using a spray gun. The MXene loading was controlled at 0.8 mg cm^{-2}, as determined by gravimetric measurement of the fabric before and after spraying on three independently prepared samples. (Figure 1b). Consequently, an integrated functional textile featuring a Janus architecture was successfully obtained.

2.4. Performance Characterization Morphology and Structural Characterization

Scanning electron microscopy (SEM, ZEISS Sigma 360, Oberkochen, Germany) and transmission electron microscopy (TEM, Hitachi HT700, Tokyo, Japan) were employed to observe the core shell structure of microcapsules and the cross-sectional morphology of the textiles. Fourier transform infrared spectroscopy (FTIR, Nicolet iS10, Thermo Fisher Scientific, Waltham, MA, USA) and X-ray photoelectron spectroscopy (XPS, Smart Lab 3KW, Rigaku, Tokyo, Japan) were utilized to analyze the chemical composition. Thermal property testing: Differential scanning calorimetry (DSC, DSC250, TA Instruments, New Castle, DE, USA) was used to measure the phase change temperature and latent heat enthalpy of the microcapsules and textiles. Thermogravimetric analysis (TGA, TG 209 F3, NETZSCH, Selb, Germany) was performed to evaluate the thermal stability of the materials. Thermal management efficacy evaluation: An infrared thermal camera was used to record the heating and cooling curves as well as the color switching process of the textiles under simulated solar irradiation from a xenon lamp (CEL-PE300L-3A, CEAULIGHT, Beijing, China). The electrothermal response of the MXene layer was tested using a programmable direct current power supply. Electromagnetic interference shielding and wettability testing: A vector network analyzer (VNA, Keysight E5080B, Keysight Technologies, Santa Rosa, CA, USA) was used to test the electromagnetic interference shielding effectiveness including total shielding effectiveness (SET), absorption shielding effectiveness (SEA) and reflection shielding effectiveness (SER) in the frequency range of 8.2 to 12.4 GHz. A contact angle measuring instrument (Attension Theta, Biolin Scientific AB, Gothenburg, Sweden) was used to evaluate the wettability and self-cleaning ability of the textiles toward water and various liquid contaminants. Multiple repetitions of each quantitative test were performed to ensure data reproducibility. Water contact angle tests were measured at five different positions on the samples while differential scanning calorimetry as well as electromagnetic interference shielding effectiveness and electrothermal response tests were based on three independently prepared samples. Experimental results are reported as the mean value plus or minus the standard deviation. A complete statistical summary of all quantitative measurements is provided in Table S1.

3. Results

3.1. Structural Characterization of the TMs

The microscopic morphology of the microcapsules and their distribution state on the fabric surface are key factors determining the thermal management and multifunctional characteristics of the composite material. The growth evolution of the SiO_2 shell provides a profound explanation for the formation of the encapsulated architecture within the phase change materials (Figure 2a). First, in the precursor solution, TEOS undergoes hydrolysis under acidic conditions to form silanol groups, followed by dehydration and polycondensation at the emulsion interface to form a continuous and dense Si–O–Si network structure that firmly encapsulates the oil in water droplets. The construction of this inorganic shell not only provides solid mechanical support for the internal phase change core material but also significantly enhances its thermal and chemical stability. Upon investigating samples synthesized with varying core to shell mass ratios encompassing 1:0.5, 1:1, 1:2 and 1:3, it was observed that the ratio of 1:2 yielded the most superior morphological integrity (Figure S2). SEM images reveal that the TMs exhibit a regular spherical structure with a smooth surface and no obvious collapse (Figure 2b,c). Statistical results indicate that the average particle size of the TMs is approximately 2 μm with a narrow size distribution, and such high uniformity is conducive to their stable dispersion within the PDMS matrix. To further investigate the internal structure and the integrity of the core shell architecture, transmission electron microscopy analysis was performed. The TMs exhibit a clear and well-defined core shell structure, where the thickness of the inorganic SiO_2 shell is approximately 20 nm (Figure 2d). This convincingly demonstrates that the SiO_2 shell has been successfully and continuously coated on the surface of the core material, providing a reliable barrier for the phase change material and preventing material leakage caused by phase transitions during temperature changes.

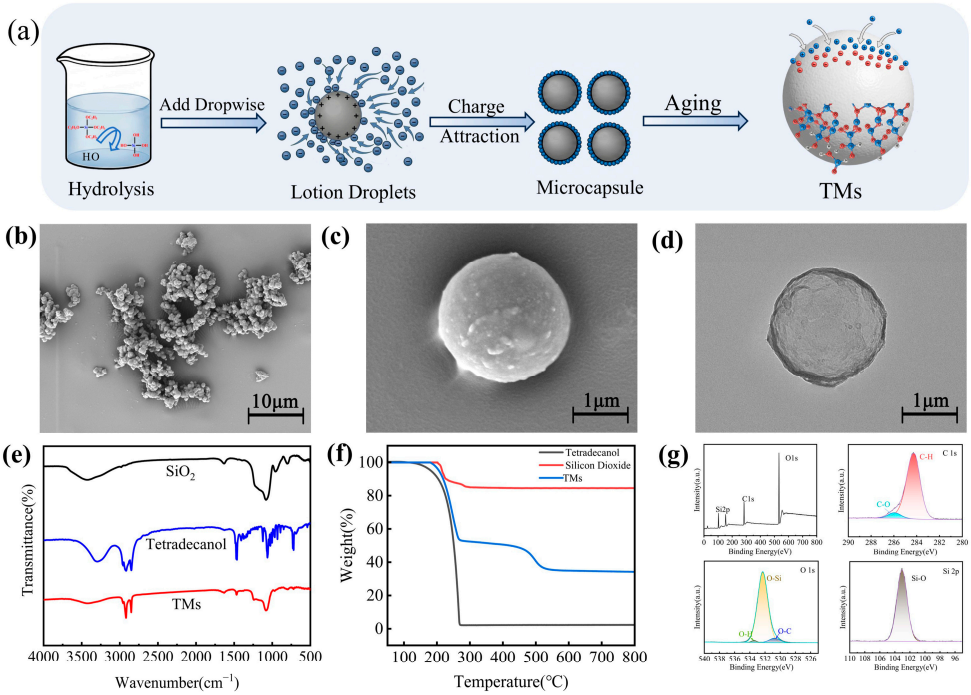


Figure 2. (**a**) Schematic illustration revealing the formation mechanism of the TMs fabricated via a sol gel method; (**b**,**c**) SEM images displaying the surface morphology of the TMs; (**d**) TEM image of the TMs highlighting the well-defined core shell architecture; (**e**) FTIR spectroscopy spectra for the chemical structural analysis of the TMs; (**f**) TGA curves evaluating the thermal stability of the individual components within the TMs; (**g**) XPS spectra identifying the elemental composition and chemical states of the TMs.

To verify the chemical composition and encapsulation effect of the TMs, the FTIR spectra of the raw materials and products were tested (Figure 2e). For 1-tetradecanol acting as the phase change material, a distinct –OH stretching vibration peak is observed at 3320 cm^{-1}, while characteristic symmetric and asymmetric stretching vibration peaks of $–CH_2–$ and $–CH_3–$ appear at 2920 cm^{-1} and 2850 cm^{-1}. A typical Si–O–Si antisymmetric stretching vibration peak of SiO_2 appears at 1080 cm^{-1}, confirming the formation of the inorganic network structure. The spectrum of the TMs retains both the aliphatic hydrocarbon characteristic peaks of 1-tetradecanol and the silicon oxygen bond characteristic peaks of SiO_2 without significant shifts or new peaks, which strongly proves the successful physical encapsulation of the 1-tetradecanol core by the SiO_2 shell while maintaining chemical structural stability during the composite process. Thermal stability is a critical parameter for evaluating the service life of phase change materials. The thermal stability of pure SiO_2, 1-tetradecanol, and TMs was evaluated via thermogravimetric analysis (Figure 2f). The results show that the pure core material begins to degrade sharply at 180 °C and completely volatilizes at 250 °C, exhibiting low thermal stability. In contrast, the SiO_2 encapsulated TMs demonstrate a distinct two stage thermal degradation characteristic, with the onset temperature of weight loss significantly shifted toward higher temperatures by approximately 20 °C compared to the pure core material. This significant thermal lag effect confirms that the dense inorganic shell acts as a physical barrier by increasing the heat conduction path and the mass transfer resistance of degradation products, effectively inhibiting the thermal escape of the core material. The second stage of weight loss above 300 °C is attributed to the further dehydration and condensation of Si–OH groups within the shell, which is highly consistent with the evolution of the silicon oxygen network observed in the FTIR. The encapsulation by the inorganic shell significantly broadens the stable working window of the core material, ensuring that the composite textile maintains excellent structural integrity and functional durability during subsequent screen printing and the active electrothermal heating process driven by the MXene layer.

XPS was employed to analyze the chemical composition and elemental distribution of the microcapsules and the coating (Figure 2g). From the wide scan spectra, characteristic peaks of C, O, and Si elements are clearly observed, indicating that the surface is primarily composed of these elements. Subsequently, high resolution fitting analysis of the C, O, and Si spectra was performed to obtain information regarding chemical bonds. The high-resolution C spectrum can be fitted into two peaks corresponding to C–H at 284.8 eV and C–O at 288 eV. The high-resolution O spectrum can be fitted into three peaks corresponding to O–Si at 532 eV, O–H at 533 eV, and O–C at 531 eV. The high-resolution Si spectrum can be fitted into one peak corresponding to Si–O at 103 eV. The XPS results corroborate the FTIR findings, confirming the chemical components of the microcapsules and the successful construction of the SiO2 shell at the atomic level, providing an important basis for revealing the thermal stability and protection mechanisms.

3.2. Characterization of Self-Adaptive Color Changing Energy Storing Multifunctional Textiles

To construct a composite system featuring efficient latent heat energy storage and sensitive thermal response characteristics, this study first prepared TMs consisting of 1-tetradecanol encapsulated in SiO_2 via a sol gel method. Figure 3a–c display the cross-sectional SEM of the FC-TMs. The Janus structure of the fabric is clearly observable from the cross section, where the upper surface is covered with a dense PDMS composite coating containing uniformly embedded TMs, while the lower surface is attached with a thin and continuous layer of MXene nanosheets. This asymmetric structural design establishes the spatial foundation for achieving active and passive dual modal thermal management. The energy dispersive spectroscopy element mapping further confirms the

uniform distribution of C, O, and Si elements within the TMs, indicating that the growth of SiO_2 on the microcapsule surface possesses a high degree of uniformity (Figure 3d).

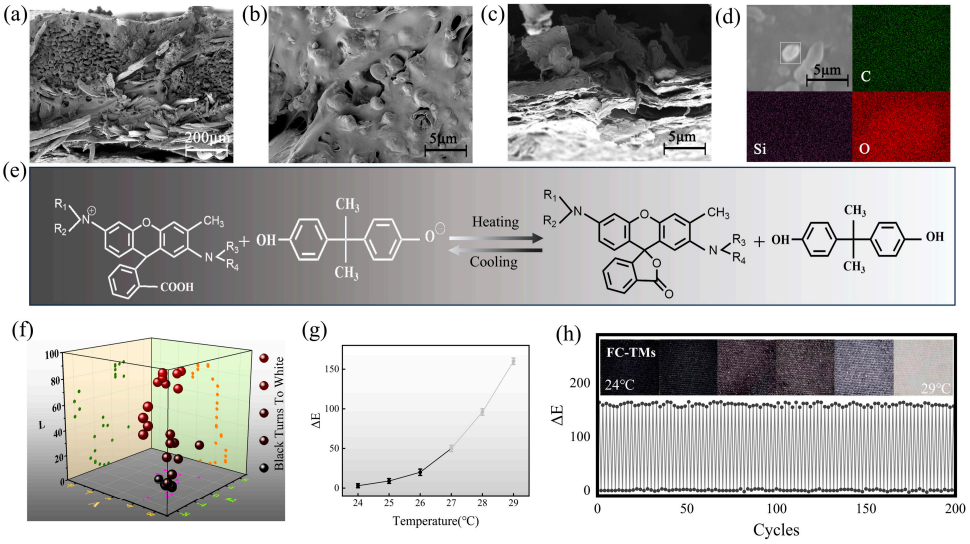


Figure 3. (**a**) SEM image of the cross section of the FC-TMs; (**b**) SEM image of the upper layer in the cross section of the FC-TMs; (**c**) SEM image of the lower layer in the cross section of the FC-TMs; (**d**) Energy dispersive spectroscopy element mapping of the TMs within the FC-TMs; (**e**) Electron transfer color changing mechanism of the thermochromic system; (**f**) CIELAB color space coordinate plots illustrating the dynamic evolution of the composite materials with temperature; (**g**) Total color difference as a function of temperature averaged over three independent measurements with error bars representing the standard deviation; (**h**) Color difference cycling tests and optical photographs of the textiles at various temperatures for comparison.

As illustrated in Figure 3e, the thermochromic system operates based on the electron transfer principle. At low temperatures, the color former and the color developer undergo electron interaction within the solvent matrix, leading to the cleavage of the lactone ring and the formation of a conjugated structure, which manifests as a deep black color. As the temperature rises above the melting point of the solvent, the color developer and color former dissociate, causing the system to revert to a colorless state and revealing the original white color of the substrate. Physical photographs intuitively record this process, showing that the thermochromic powder undergoes a sensitive transition from black to white as the temperature crosses the phase change interval.

The color transition process was quantitatively characterized using CIELAB color space plots in Figure 3f. The results demonstrate that as the temperature increases, the L* value representing lightness significantly increases from 1 to 84, while both the red–green axis A* and the yellow–blue axis B* approach the origin. This significant color shift confirms the application potential of these microcapsules in the fields of smart temperature control and visual camouflage. Figure 3g presents the temperature-dependent total color difference averaged over three independent measurements with error bars representing the standard deviation. The ΔE–temperature curves exhibit a well-defined sigmoidal transition, and the small standard deviations across the measured temperature range confirm the high repeatability of the thermochromic response. Figure 3h illustrates the color cycling test of the functional composite textiles. After 200 continuous cycles, the color difference value of the fabric consistently remains at approximately 160 ± 5, proving that the coating possesses excellent color cycling durability. Physical photographs further verify this process, as the coating undergoes a sensitive and reversible switch from black to white whenever the temperature crosses the phase change threshold.

3.3. Phase Change Energy Storage and Passive Photothermal Management

Figure 4a illustrates the DSC curves of the microcapsules during the heating and cooling processes. In the heating curve, a distinct endothermic peak is observed with a melting peak temperature Tm of approximately 41 °C and a mean melting enthalpy ΔHm of 121 ± 4 J g^{-1}. In the cooling curve, the crystallization temperature Tc of the exothermic peak is 31 °C with a mean crystallization enthalpy ΔHc of 122 ± 3 J g^{-1}. Based on the melting enthalpy of the pure 1-tetradecanol core measured under identical DSC conditions (231 J g^{-1}), the encapsulation efficiency was calculated to be 52.3 ± 0.9%. This efficiency is consistent with the well-defined core–shell structure observed in TEM imaging and confirms effective encapsulation of the alkane core by the SiO_2 shell. These results indicate that the microcapsules possess high latent heat values and reliable encapsulation performance, verifying that the dense SiO_2 shell effectively seals the 1-tetradecanol core material and prevents leakage during repeated thermal cycling. This architecture enables stable energy absorption and release under atmospheric conditions, thereby mitigating temperature fluctuations on the textile surface. To explore the dynamic radiative regulation capability of the fabric, the ultraviolet visible near infrared spectra were measured under different states. In the low temperature black state (Figure 4b), the textile exhibits extremely high absorption across the entire spectrum, which is conducive to maximizing the capture of solar radiative energy and converting it into thermal energy for passive heating. When the ambient temperature rises above the transition threshold, the thermochromic system switches from black to white (Figure 4c). At this point, the reflectance of the textile in the visible and near infrared regions increases significantly, effectively blocking further solar input. This cold and hot self-switching optical characteristic endows the textile with the ability to intelligently perceive environmental radiation, achieving an adaptive balance of human thermal comfort under varying climatic conditions.

The photothermal performance of the composite textiles in practical working scenarios was further evaluated using a simulated solar light source and an infrared thermal camera (Figure 4d). Figure 4e records the dynamic evolution of three comparative samples during the heating process. The white textile coated only with TMs (left) shows the lowest photothermal conversion efficiency and a gentle heating curve due to its extremely high solar reflectance. In contrast, the pure black textile (right) exhibits a rapid and continuous temperature rise, which easily leads to an overheating risk and a sharp temperature drop after the light source is turned off, indicating a lack of sustained thermal stability. The adaptive thermochromic composite textile (middle) demonstrates a unique active and passive synergetic regulation logic. In the initial phase, the textile in the black state rapidly absorbs light energy to achieve fast heating. When the temperature reaches the color change point, the surface transforms to white to enhance solar radiation reflection, thereby effectively suppressing excessive temperature increases, a phenomenon known as overheating inhibition. This phase can be designated as the dynamic regulation stage. Subsequently, the process enters the thermal buffering stage, where a prominent plateau is observed in the temperature rise curve, attributed to the latent heat absorption of the TMs. Finally, once the light source is extinguished, the microcapsules release their stored latent heat, causing the temperature to decrease at a rate significantly slower than that of the pure black textile, thereby entering the heat retention stage. Figure 4f–h display the temperature evolution curves over time under different solar radiation intensities of 0.5, 1, and 2 Suns. The results confirm that the composite textile can stabilize the temperature within the human comfort zone through the synergy of optical regulation and phase change energy storage in both low light and strong light environments. Under low light, the surface temperature rises slowly and maintains appropriate comfort. Upon entering a strong light environment, the adaptive textile absorbs solar light and the phase change material

absorbs heat to undergo a phase transition, leading to a rapid color change from deep black to white. This decrease in solar absorption rate causes the surface temperature to rise slowly, achieving adaptive thermal comfort transformation in high temperature and high light environments. When the illumination ceases, the TMs release the stored latent heat, causing the temperature cooling rate to be significantly lower than that of the pure black textile. This all-weather adaptive capability demonstrates the application value of these FC-TMs in thermal management for extreme environments such as field tents and smart protective clothing. Notably, the thermochromic switching temperature of the coating is approximately 29 °C. When the textile surface approaches this temperature under sunlight, the coating rapidly transitions from black to white, thereby increasing solar reflectance and suppressing the initial overheating tendency. At this stage, the 1-tetradecanol core encapsulated within the SiO_2 shell remains in the solid state and contributes negligible latent heat. As environmental heating persists and radiative modulation alone becomes insufficient, the TMs reach their melting onset at approximately 41 °C and begin to absorb a substantial amount of latent heat, forming a high-enthalpy thermal buffer. This sequential mechanism—low-energy optical modulation followed by high-capacity phase-change heat storage—avoids premature energy dissipation and achieves a staged, smooth response to temperature fluctuations. This stepwise logic ensures that under mild overheating, the textile relies primarily on optical regulation without prematurely consuming the phase-change material, and activates substantial heat absorption only under more intense thermal stress, thereby maintaining thermal comfort.

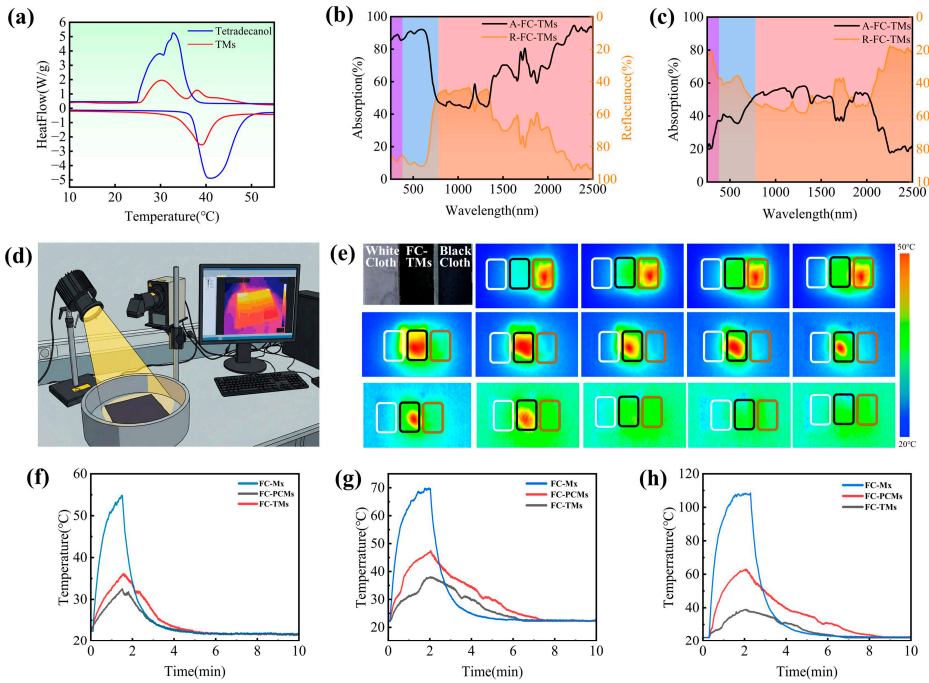


Figure 4. (**a**) DSC curves of pure 1-tetradecanol and silica encapsulated TMs, demonstrating their phase change enthalpy and thermal energy storage characteristics. (**b**,**c**) Ultraviolet visible near infrared absorption and reflection spectra of the functional composite textiles in (**b**) the low temperature black state and (**c**) the high temperature white state, representing their dynamic optical modulation capability. (**d**) Schematic illustration of the experimental setup and principles for photothermal conversion and infrared thermal imaging tests under a simulated solar light source. (**e**) Dynamic infrared thermal images of three typical samples including pure phase change microcapsule coating and FC-TMs and pure black fabric during simulated solar irradiation and after the light source was extinguished. (**f**–**h**) Surface temperature evolution curves over time for the three samples under solar radiation intensities of (**f**) 0.5 Sun and (**g**) 1 Sun and (**h**) 2 Suns, revealing the self-adaptive temperature regulation and thermal buffering mechanisms of the textiles.

3.4. Multifunctional Applications

To achieve on demand thermal supplementation in extreme cold environments, this study utilized the MXene coating on the back of the fabric to endow the FC-TMs with excellent active electrothermal functions. Figure 5a displays the optical photographs and corresponding infrared thermal images of the electrothermal tests. The results show that the textile surface temperature rises rapidly and uniformly when a low driving voltage is applied, and no obvious local hot spots are observed at thermal equilibrium, confirming that the MXene nanosheets have constructed a highly continuous and uniform conductive network on the textile fiber surfaces. Figure 5b records the temperature rise curves of the textile over time under different driving voltages of 3 V, 4 V, and 5 V. According to Joule's law, the steady state temperature exhibits a significant voltage dependence. When the voltage increases from 3 V to 5 V, the temperature can rise from 40 °C to 65 °C within 1 min, demonstrating an extremely fast thermal response speed. For wearable or flexible outdoor equipment, electromechanical stability is of paramount importance. The electro-thermal cycling stability of the textile was evaluated over 100 cycles at 3 V, 4 V, and 5 V (Figure 5c). The heating curves maintain a high degree of overlap across multiple cycles without obvious performance degradation, proving its ability to withstand thermal degradation and mechanical fatigue during long term service. Furthermore, Figure 5d illustrates the resistance strain tests of the textile under different bending angles. The results show that the mean relative resistance change measured on three independent samples remains within an extremely low range with a standard deviation of less than 2% during cyclic bending, indicating strong interfacial adhesion between the MXene and the textile substrate. Cyclic testing of the resistance variation was performed for 100 cycles under a bending strain of 20%. The results indicate that the mean coating resistance remains essentially stable with a standard deviation of less than 1.5%, further confirming the robust interfacial adhesion between the coating and the substrate (Figure S3).

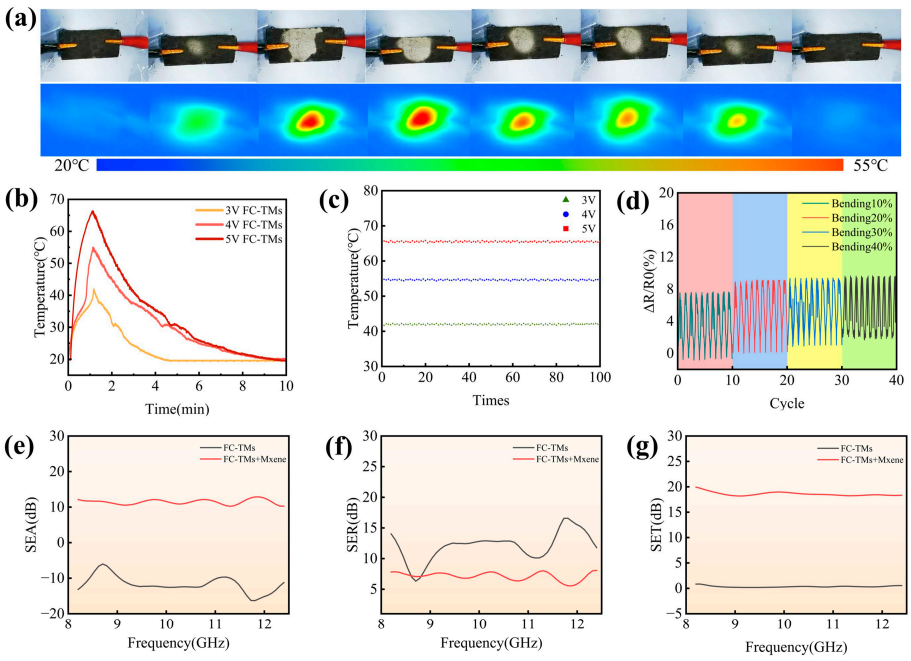


Figure 5. (**a**) Optical photographs and corresponding infrared thermal images of the textile under driving voltages; (**b**) Temperature rise response curves of the textiles under driving voltages of 3 V, 4 V and 5 V; (**c**) Electro-thermal cycling stability over 100 cycles at different voltages; (**d**) Resistance change under cyclic bending at different angles; (**e**–**g**) Electromagnetic interference shielding performance encompassing total, absorption, and reflection shielding effectiveness of the composite textiles in the X band.

Attributed to the electrical conductivity and the unique multi layered stacking architecture of the back side transition metal carbide layer, the functional composite textiles exhibit effective electromagnetic interference shielding performance and infrared stealth characteristics as displayed in Figure S4. Figure 5e–g demonstrate the shielding effectiveness of the textiles in the X band ranging from 8.2 to 12.4 GHz. The results show that the mean total shielding effectiveness, measured on three independently prepared textile samples, reaches 20 dB with a standard deviation of approximately 0.8 dB, meeting the standard for commercial applications. Through an in-depth analysis of the shielding mechanism, it was found that absorption loss dominates the total shielding effectiveness. This is attributed to the multiple reflections and scattering of incident electromagnetic waves by the MXene layer as well as the conductive loss of internal carriers within the MXene under an alternating electromagnetic field. This shielding mechanism dominated by absorption can effectively prevent secondary electromagnetic pollution, suggesting potential applications in fields such as electronic countermeasures, advanced protection, and smart cabins.

The ambient stability of the MXene layer was assessed by monitoring the electrical resistance and the electromagnetic interference shielding effectiveness of the spray-coated back surface under laboratory storage conditions over a period of two weeks. After 14 days of exposure to ambient air, the electrical resistance increased by approximately 30% and the EMI shielding effectiveness decreased by approximately 14%, confirming progressive partial oxidation of the $Ti_3C_2T_x$ nanosheets, a behavior well documented for MXene coatings stored without protective encapsulation. In the present Janus configuration, the dense PDMS front layer and the compact cotton fabric substrate serve as partial physical barriers that limit the ingress of oxygen and moisture from the external environment toward the interior-facing MXene network, thereby slowing the oxidation rate relative to that expected for a fully exposed MXene coating. Nevertheless, this passive protection alone is insufficient to preserve the long-term conductivity and shielding performance required for multi-month outdoor service. Future development of the textile for extended deployment should therefore incorporate dedicated stabilization measures, such as a thin polymeric or inorganic overcoat directly on the MXene layer, surface passivation treatments, or the addition of antioxidant additives to the MXene dispersion before spraying. These strategies have been demonstrated in the MXene literature to significantly retard oxidative degradation and would be essential to translate the current Janus textile into a durable outdoor product [49].

3.5. Multi-Functional Expansion

The synergistic effect of micro and nano scale rough structures and low surface energy substances is critical for constructing the hydrophobic characteristics of functionalized textiles. As illustrated in Figure 6a, the mean static water contact angle measured at five independent positions on the functional composite textile surface is 130.2° with a standard deviation of 2.5°, demonstrating significant hydrophobic characteristics primarily attributed to the hierarchical micro and nano scale structures constructed by the PDMS matrix and the phase change TMs. To verify the durability in actual outdoor service environments, self-cleaning performance tests were conducted (Figure 6b). When the textile surface is covered with dust acting as a simulated pollutant, water droplets roll off under the influence of gravity and rapidly carry away surface contaminants. This excellent self-cleaning capability not only prevents interference from rainwater or stains on the optical regulation performance of the textile but also ensures the structural integrity and functional stability of the functional coating during long term outdoor use.

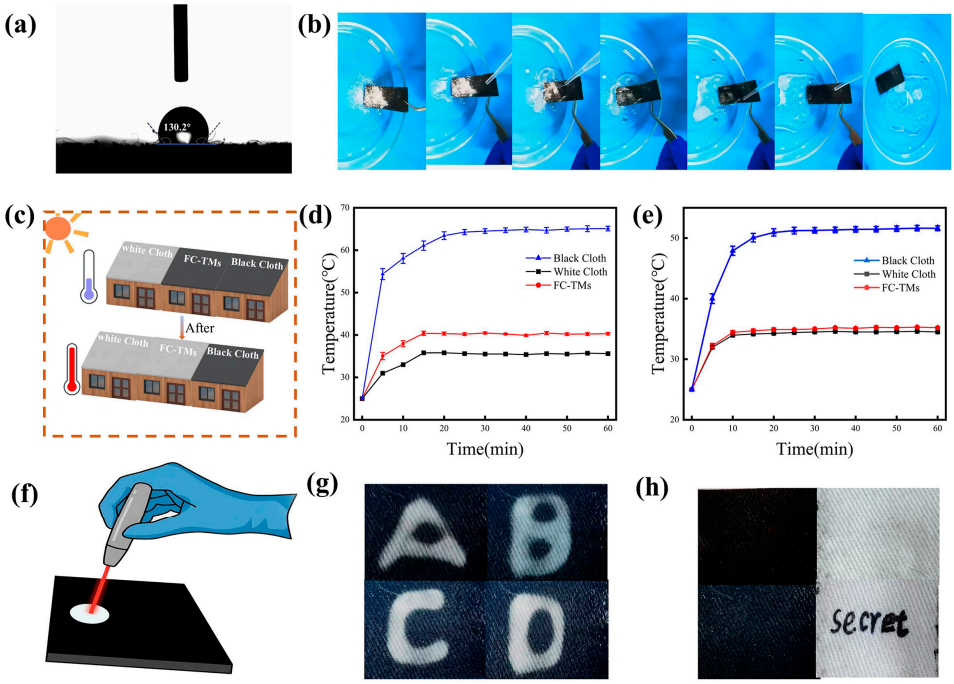


Figure 6. (**a**) Static water contact angle measurements of the functional composite textiles demonstrate their hydrophobic characteristics; (**b**) Optical photographs capturing the self-cleaning process of contaminants on the textile surface; (**c**) Thermal management testing scenario of the outdoor architectural model under natural sunlight; (**d**,**e**) Dynamic temperature evolution curves of the (**d**) surface and (**e**) interior of the model under a radiation intensity of 0.76 Sun. Data points represent the mean of three replicate readings taken at 5 min intervals; error bars denote the standard deviation. Adjacent points are connected by straight lines without any smoothing; (**f**) Schematic illustration of the irradiation process using a handheld near infrared lamp; (**g**) Demonstration of non-contact information display achieved via the near infrared photothermal conversion effect; (**h**) Application demonstration of encrypted information hiding and thermal revealing based on the thermochromic characteristics.

The washing durability of the Janus textile was evaluated over six laundering cycles. On the front surface, the static water contact angle was 128 ± 1.7° after six washes, compared with 130.2 ± 2.5° before washing, indicating no statistically significant deterioration in water repellency. The thermochromic color change behavior also remained essentially unchanged, with the color difference after six cycles retaining a value of approximately 158 ± 4. In contrast, the MXene-coated back surface, which was deposited by direct spray coating without a protective overcoat, suffered a near-complete loss of electrical conductivity after six washing cycles. This pronounced degradation is attributed to the weak adhesion of the MXene nanosheets to the cotton substrate under mechanical agitation and their susceptibility to oxidation upon water immersion, leading to extensive detachment and disruption of the conductive network. However, in the intended application configuration the MXene layer constitutes the interior face of the textile while the hydrophobic PDMS front faces outward. This Janus architecture prevents liquid penetration through the fabric cross section, thereby shielding the MXene back layer from direct contact with water and detergents during use and mild cleaning. Consequently, the PDMS front provides inherent passive protection for the conductive back layer, although the development of dedicated encapsulation or lamination strategies for the MXene network remains necessary for applications demanding rigorous machine laundering on a regular basis.

To further evaluate the application potential of the FC-TMs under actual complex climatic conditions, an outdoor architectural model was constructed and subjected to field exposure tests (Figure 6c). The outdoor experiment was performed on 25 September 2025, from 12:30 to 13:30 local time, at Qingdao University, Qingdao, China (36.06° N, 120.38°

E; altitude approximately 15 m). The weather was clear with full sunshine, an ambient temperature of 28 ± 1 °C, and a relative humidity of approximately 48%. The average solar irradiance during the measurement period was 0.76 Sun (approximately 760 W/m^2), as recorded by a calibrated pyranometer. Under a continuous natural sunlight exposure of 1 h, the temperature evolution of the model surface and interior was monitored in real time. Temperatures were manually recorded at 5 min intervals. At each time point, three rapid consecutive readings were taken and the mean ± standard deviation was calculated. Figure 6d illustrates the temperature curve of the model surface, where each data point represents the mean of three replicate readings and error bars denote the standard deviation. Since the thermochromic layer appears black in the initial low temperature state, the textile rapidly absorbs solar radiation leading to a temperature rise. As the temperature crosses the phase change threshold, the textile automatically switches to a high reflection white state, which effectively inhibits further heat accumulation and presents a significant overheating inhibition characteristic. Meanwhile, the internal temperature curve (Figure 6e) is presented in the same manner with mean ± SD from triplicate readings. It demonstrates stability with a heating rate far lower than that of the surface environment. This is credited to the synergistic effect of the latent heat buffering from the upper layer and the radiative regulation of the color changing layer, which successfully blocks external thermal intrusion and creates a constant microclimate for the internal space. The small error bars observed across all time points indicate excellent short-term measurement precision and confirm the high reliability of the manual infrared temperature readings. This adaptive thermal management capability highlights its application potential in multifunctional field tents and specialized protective clothing.

The functional composite textiles also exhibit sensitive near infrared light thermal response characteristics (Figure 6f). A handheld near infrared lamp was used for local irradiation of the textile. Owing to the efficient photothermal conversion efficiency of the MXene layer and the microcapsule components, the light receiving area can undergo rapid color switching. Figure 6g demonstrates the photothermal display effect achieved on the textile surface using a near infrared beam. This non-contact optical induction color change provides a new pathway for flexible displays and dynamic camouflage. Figure S5 presents the optical images and infrared thermal images under near infrared beam irradiation. The white regions represent the heated areas while the black portions indicate low temperature regions, corresponding to the red and blue sections in the infrared images, respectively.

Furthermore, advanced information encryption and security applications can be realized by utilizing the thermochromic characteristics of the textile. As illustrated in Figure 6h, specific information was written on the initially black textile surface using a black marker. At room temperature, the information exhibits excellent concealment due to the lack of background contrast. Upon heating, the textile substrate transforms from black to white while the ink remains dark, allowing the hidden information to be clearly revealed. This encryption logic based on temperature-controlled contrast switching demonstrates unique application advantages in the fields of anti-counterfeiting labels and confidential information transmission. It should be noted that the continuous PDMS coating on the front surface, although essential for hydrophobicity, self-cleaning, and phase-change material encapsulation, inherently reduces air and moisture vapor permeability. This represents a deliberate trade-off in the current Janus design, where environmental protection and durable thermal regulation are prioritized over passive moisture transport. Such a configuration is well suited for field tent fabrics, outer shells of protective suits, and equipment covers, as these applications equally demand windproofness and liquid repellency while allowing moisture dissipation through garment openings or ventilation design. For applications requiring both high breathability and thermal management, such as next-to-skin

sportswear, future iterations may incorporate patterned coatings, hydrophilic modification of the PDMS layer, or breathable membrane substrates, thereby preserving the multifunctional advantages without compromising wearer comfort. The focus of the present study is the realization of synergistic active and passive thermal management together with electromagnetic interference shielding on a single textile platform.

To further clarify the position of the present work within the existing literature, Table 1 provides a quantitative comparison of the FC-TMs Janus coating with representative multifunctional thermal management coatings and textiles reported recently. Compared with existing thermal management coating systems, the present work integrates passive radiative regulation, active Joule heating, and electromagnetic interference shielding on a single fabric platform through a Janus architecture, offering a distinct advantage in terms of functional completeness.

Table 1. Comparison of the present FC-TMs Janus coating with representative multifunctional thermal management coatings and textiles reported in the recent literature.

Property	Ref. [26] (Zhu et al., 2024)	Ref. [7] (Xue et al., 2023)	Ref. [13] (Liu et al., 2024)	This Work (FC-TMs)
Material system	rGO-wrapped thermochromic PCM microcapsules plus $BaSO_4$ spray-coated on polyester fabric	CNT-doped thermochromic microcapsules plus graphene conductive back layer coated on cotton	Thermochromic microcapsules mixed in PDMS elastomer coating	Janus architecture with PCM/thermochromic PDMS front and MXene conductive back on cotton
Passive radiative regulation	Yes black/white switching ~80% visible modulation emissivity 0.94 in atmospheric window	Yes blue/white switching 30–35 °C range	Yes black/white switching with phase-change heat storage	Yes black/white switching plus high-enthalpy latent heat buffering via sequential triggering
Active Joule heating	No	Yes graphene layer ~45 °C at 6 V	Not reported	Yes MXene layer 40–65 °C at 3–5 V
EMI shielding	Not reported	Not reported	Not reported	Yes SET 20 dB absorption-dominated
Latent heat	~100 J g^{-1}	70.6 J g^{-1}	~82.8 J g^{-1} core/shell ratio 5:1	121 ± 4 J g^{-1}
WCA	Not reported	Not reported	Not reported	130.2 ± 2.5°
Color-change cycles	25 cycles	500 cycles	25 cycles	200 cycles
Fabrication method	Spray coating + UV reduction	In situ polymerization plus screen printing plus coating	Solvent evaporation plus PDMS blending and curing	Sol-gel plus screen printing front plus spray coating back

4. Conclusions

In summary, this research successfully constructed a Janus structured smart textile integrating SiO_2 encapsulated TMs and thermochromic microcapsules as well as MXene nanosheets through a combination of sol gel and screen printing and spray coating techniques. Systematic characterization confirmed that the TMs possess a robust core shell structure and excellent thermal stability, which effectively prevents the leakage of phase change materials and ensures structural integrity throughout complex clothing application environments. By synergistically integrating the self-adaptive color switching and latent heat buffering mechanisms on the front surface with the high efficiency active electrothermal heating function on the back, the composite textile achieves a synergistic interaction of multiple thermal regulation mechanisms. This design not only maintains human thermal comfort under intense environmental temperature fluctuations but also endows the textile with electromagnetic interference shielding effectiveness dominated by conduction loss alongside biomimetic hydrophobic self-cleaning properties. This integration strategy,

which combines energy storage and color changing adaptability with electromagnetic protection and environmental endurance, provides an effective self-adaptive strategy for developing high-performance outdoor protective gear, equipment covers, and multifunctional all-weather field tents. With further optimization of moisture permeability and wash durability, it also holds promise for extending to smart protective clothing.

Supplementary Materials: The following supporting information can be downloaded at: https://www.mdpi.com/article/10.3390/coatings16050583/s1, Figure S1: Schematic illustration of the fabrication processes for the TMs microcapsules and the Janus-structured multifunctional textile.; Figure S2: SEM images of TMs microcapsules prepared with different core-to-shell mass ratios: (a) 1:0.5, (b) 1:1, (c) 1:2, and (d) 1:3.; Figure S3: Electromechanical durability of the MXene-coated layer on the Janus textile. Dynamic resistance (R) variation during 100 continuous bending-releasing cycles at a constant bending strain of 20%, demonstrating the robust interfacial adhesion and structural stability of the conductive network.; Figure S4: Demonstration of infrared (IR) stealth and thermal camouflage performance of the MXene-coated Janus textile. (a) Optical photograph (left) and corresponding IR thermal image (right) of the MXene layer and ordinary cotton cloth placed on an ambient background. (b) Optical photograph (left) and corresponding IR thermal image (right) of the MXene layer covering a human hand, showcasing the effective masking of human thermal radiation.; Figure S5: Demonstration of remote NIR-responsive photothermal patterning and information display on the FC-TMs. (a–d) Sequential digital photographs (top) and corresponding infrared (IR) thermal images (bottom) showcasing the letters "A", "B", "C", and "D" drawn on the fabric surface using a near-infrared spotlight.; Table S1: Statistical summary of key quantitative measurements.

Author Contributions: Q.L.: Conceptualization, Methodology, and Writing—Original Draft Preparation; H.L.: Validation, Data Curation, and Writing—Original Draft Preparation; H.W.: Validation, Data Curation, and Writing—Original Draft Preparation; Z.Z.: Validation, Data Curation, and Writing—Original Draft Preparation; W.C.: Validation and Writing—Original Draft Preparation; Y.Y.: Methodology and Data Curation; L.L.: Validation and Data Curation; X.W.: Supervision and Writing—Review and Editing; X.Z.: Writing—Review and Editing and Funding Acquisition. All authors have read and agreed to the published version of the manuscript.

Funding: This research was supported by the National Natural Science Foundation of China (No. 42476227), Key R&D Program of Shandong Province, China (No. 2025JMRH0202), China Postdoctoral Science Foundation (No. 2023M731838 and No. 2024T170446), and Qingdao Natural Science Foundation (No. 24-4-4-zrjj-197-jch).

Institutional Review Board Statement: Not applicable.

Informed Consent Statement: Not applicable.

Data Availability Statement: The original contributions presented in this study are included in the article. Further inquiries can be directed to the corresponding author.

Acknowledgments: We would like to acknowledge all the staff that participated in this study. During the preparation of this manuscript, the author used [Gemini AI Tools] for the purposes of [Figure 1 and Figure S1]. The authors have reviewed and edited the output and take full responsibility for the content of this publication.

Conflicts of Interest: Authors Lili was employed by the company Shaanxi Yuanfeng Prosafe Co., Ltd. The remaining authors declare that the research was conducted in the absence of any commercial or financial relationships that could be construed as potential conflicts of interest.

References

1. Shooshtarian, S. Theoretical dimension of outdoor thermal comfort research. *Sustain. Cities Soc.* **2019**, *47*, 101495. [CrossRef]
2. He, M.; Zhao, B.; Yue, X.; Chen, Y.; Qiu, F.; Zhang, T. Infrared radiative modulating textiles for personal thermal management: Principle, design and application. *Nano Energy* **2023**, *116*, 108821. [CrossRef]

3. Gu, B.; Dai, Z.; Pan, H.; Zhao, D. Integration of prolonged phase-change thermal storage material and radiative cooling textile for personal thermal management. *Chem. Eng. J.* **2024**, *493*, 152637. [CrossRef]
4. Pu, Y.; Fan, J. Thermoresponsive Skin-like Fabric for Personal Comfort and Protection. *ACS Appl. Mater. Interfaces* **2024**, *16*, 10960–10968. [CrossRef]
5. Zhang, W.; Zhang, H.; Liu, S.; Zhang, X.; Li, W. Preparation and crystallization behavior of sensitive thermochromic microencapsulated phase change materials. *Appl. Energy* **2024**, *362*, 122993. [CrossRef]
6. Ge, F.; Yu, W.; Yin, Y.; Wang, C. Solar-driven thermochromic fabric based on photothermal conversion for light intensity monitoring. *J. Mater. Chem. A* **2021**, *9*, 20565–20575. [CrossRef]
7. Xue, D.; Zhao, T. The electrothermal color-changing fabric based on high-sensitivity thermochromic microcapsules. *Colloids Surf. A Physicochem. Eng. Asp.* **2023**, *678*, 132458. [CrossRef]
8. Sudharshan Reddy, P.; Umer, S.; Buhari, D. The role of environmental technology for energy demand and energy efficiency: Evidence from OECD countries. *Renew. Sustain. Energy Rev.* **2021**, *153*, 111735. [CrossRef]
9. Zhang, Y.; Liu, H.; Niu, J.; Wang, X.; Wu, D. Development of reversible and durable thermochromic phase-change microcapsules for real-time indication of thermal energy storage and management. *Appl. Energy* **2020**, *264*, 114729. [CrossRef]
10. Ge, F.; Yu, W.; Zhang, W.; Yin, Y.; Wang, C. Sunlight-Responsive Photothermochromic Fabric with Reversible Color Changing Based on Photothermal Conversion. *Sol. Rrl* **2021**, *5*, 2100135. [CrossRef]
11. Geng, X.; Gao, Y.; Wang, N.; Han, N.; Zhang, X.; Li, W. Intelligent adjustment of light-to-thermal energy conversion efficiency of thermo-regulated fabric containing reversible thermochromic MicroPCMs. *Chem. Eng. J.* **2020**, *408*, 127276. [CrossRef]
12. Wang, C.; Wang, J.; Zhang, L.; Fu, S. Solar-driven bistable thermochromic textiles based on supercooling and space constraint anchoring electron transfer. *J. Mater. Chem. A* **2023**, *11*, 10798–10806. [CrossRef]
13. Liu, Y.; Wu, Y.; Ma, Y.; Wang, P.; Yu, B.; Pei, X.; Liu, S.; Zhou, F. Reversible thermochromic and heat storage coating for adaptive de/anti-icing and thermal regulation. *Chem. Eng. J.* **2024**, *482*, 148837. [CrossRef]
14. Wang, M.; Yang, T.; Cao, G.; Wang, X.; Jiang, Z.; Wang, C.; Li, Y. Simulation-guided construction of solar thermal coating with enhanced light absorption capacity for effective icephobicity. *Chem. Eng. J.* **2020**, *408*, 127316. [CrossRef]
15. Deng, G.; Yang, Y.; Lu, S.; Ma, L.; Wu, G. Silk Fabrics Modified with Photothermal Phase Change Microcapsules for Personal Thermal Management. *Int. J. Nanomed.* **2024**, *19*, 8485–8499. [CrossRef]
16. Liu, H.; Jiang, M.; Geng, S.; Liu, X. Modulation of an Si-O-Si structure in uniformly photochromic microcapsules for solar heat and daylight management. *Chem. Eng. J.* **2024**, *490*, 151545. [CrossRef]
17. Zhang, Q.; Cheng, H.; Zhang, S.; Li, Y.; Li, Z.; Ma, J.; Liu, X. Advancements and challenges in thermoregulating textiles: Smart clothing for enhanced personal thermal management. *Chem. Eng. J.* **2024**, *488*, 151040. [CrossRef]
18. Xu, T.; Yeow Seow, J.Z.; Tan, S.; Li, S.; Chen, T.; Ji, G.; Xu, Z.J. Radiative Smart Fibers and Textiles: Thermal Management and Beyond. *ACS Nano* **2025**, *19*, 32995–33007. [CrossRef]
19. Xue, D.; Lv, C.; Bi, X.; Wang, Y.; Chen, Z.; Zhao, T.; Li, T. Colorful thermochromic microcapsules for visual temperature sensing and moisture-thermal management. *Polymer* **2025**, *344*, 129534. [CrossRef]
20. Wu, J.; Yu, P.; Wang, L.; Zhang, X.; Xie, W.; Zeng, J.; Zhou, G.; Zhang, Z. Reversible Thermochromic Phase Change Material Microcapsules With High Latent Heat via Cellulose Nanocrystal Stabilized Pickering Emulsion for Smart Coatings. *Small* **2025**, *21*, 2505575. [CrossRef]
21. Tözüm, M.S. Double-shell microcapsules with enhanced thermal stability and low leakage for thermochromic and thermal energy storage textiles. *Cellulose* **2025**, *32*, 7445–7464. [CrossRef]
22. Liu, S.; Zhang, H.; Zhang, X.; Li, W. Reversible thermochromic microencapsulated phase change materials with silane-terminated polyurethane shell. *J. Energy Storage* **2025**, *119*, 116329. [CrossRef]
23. Zhang, J.; Zhang, Y.; Wu, S.; Ji, Y.; Mao, Z.; Wang, D.; Xu, Z.; Wei, Q.; Feng, Q. Weavable coaxial phase change fibers concentrating thermal energy storage, photothermal conversion and thermochromic responsiveness toward smart thermoregulatory textiles. *Chem. Eng. J.* **2024**, *483*, 149281. [CrossRef]
24. Lv, P.; Sheng, Y.; Xie, Y.; Hu, Y.; Wang, H.; Huo, X.; Li, X.; Qi, H.; Yu, W.; Dong, X. Electrospun Janus film: Innovative design of "macro + micro" to achieve thermochromic-anisotropic conductive-fluorescent tri-functionality. *Chem. Eng. J.* **2024**, *497*, 154820. [CrossRef]
25. Jiang, S.; Zhang, K.; Wang, C.-F.; Li, Q.; Zhu, L.; Chen, S. Recent advancements in radiative cooling textiles for personal thermal management. *J. Mater. Chem. A* **2024**, *12*, 14866–14884. [CrossRef]
26. Zhu, K.; Yao, H.; Song, J.; Liao, Q.; He, S.; Guang, T.; Wang, H.; Hao, X.; Lu, B.; Lin, T.; et al. Temperature-adaptive dual-modal photonic textiles for thermal management. *Sci. Adv.* **2024**, *10*, eadr2062. [CrossRef]
27. Ju, Y.; Lang, Z.; Wang, Y.; Xiao, Z.; Wang, H.; Xie, Y. Cellulose-based phase change membranes with reversible optical transmittance and lignin ester-enhancing photothermal conversion performance. *Chem. Eng. J.* **2023**, *469*, 143921. [CrossRef]
28. Alkan, C.; Alakara, E.H.; Alay Aksoy, S.; Demir, İ. Cement mortar composites including 1-tetradecanol@PMMA Pickering emulsion particles for thermal energy management of buildings. *Chem. Eng. J.* **2023**, *476*, 146843. [CrossRef]

29. Zhang, D.; Yang, A.-S.; Jiang, Z.; He, F.; Li, Y.; Li, X.; Chen, Z.; Yang, W. Paraffin@silica@poly(dopamine)/Silver Phase Change Microcapsules with Efficient Photothermal Conversion Performance. *Energy Fuels* **2023**, *37*, 16951–16961. [CrossRef]
30. Yuan, K.; Chen, Q.; Zhang, A.; Xiao, N.; Zou, X.; Lin, Z. Efficient thermal energy conversion and storage enabled by hybrid graphite nanoparticles/silica-encapsulated phase-change microcapsules. *J. Mater. Chem. A* **2023**, *12*, 2456–2464. [CrossRef]
31. Zhang, H.-J.; Chen, X.-H.; Wang, F.-Q.; Chen, R.-S.; Han, L. Dodecane/Silica Phase Change Microcapsules: Fabrication, Structure and Stability. *Sci. Adv. Mater.* **2023**, *15*, 887–893. [CrossRef]
32. Zhang, X.; Zuo, T.; Ai, M.; Yu, D.; Wang, W. All-in-One Cast-Molded Hydrophobic Silicon Dioxide-Phase Change Microcapsule/Gelatin-Hydroxyethyl Cellulose Composite Aerogel for Building Cooling. *ACS Sustain. Chem. Eng.* **2024**, *12*, 10423–10435. [CrossRef]
33. Tan, Y.; Li, P.; Yao, Y.; Li, H.; Zhong, J.; Wu, J.; Zhang, Y.; Wang, J. Green preparation and performance research of n-octadecane@silica phase change microcapsules for building energy conservation. *Constr. Build. Mater.* **2025**, *497*, 143847. [CrossRef]
34. Chen, Z.; Su, X.; Wu, W.; Zhou, J.; Wu, T.; Wu, Y.; Xie, H.; Li, K. Superhydrophobic PDMS@GSH wood with Joule heat and photothermal effect for viscous crude oil removal. *Carbon* **2022**, *201*, 577–586. [CrossRef]
35. Zhang, J.; Huang, Y.; Zhang, X.; Guo, X.; Chen, K.; Feng, X.; Kong, J.; Liu, Y.; Shang, B.; Xu, W.; et al. Flexible transparent and hydrophobic SiNCs/PDMS coatings for anti-counterfeiting applications. *Mater. Horiz.* **2024**, *11*, 3573–3584. [CrossRef] [PubMed]
36. Wang, M.; Zi, Y.; Zhu, J.; Huang, W.; Zhang, Z.; Zhang, H. Construction of super-hydrophobic PDMS@MOF@Cu mesh for reduced drag, anti-fouling and self-cleaning towards marine vehicle applications. *Chem. Eng. J.* **2021**, *417*, 129265. [CrossRef]
37. Kumar, R.; Sahoo, S.; Joanni, E.; Shim, J.-J. Cutting edge composite materials based on MXenes: Synthesis and electromagnetic interference shielding applications. *Compos. Part B Eng.* **2023**, *264*, 110874. [CrossRef]
38. Wang, L.; Cheng, J.; Zou, Y.; Zheng, W.; Wang, Y.; Liu, Y.; Zhang, H.; Zhang, D.; Ji, X. Current advances and future perspectives of MXene-based electromagnetic interference shielding materials. *Adv. Compos. Hybrid Mater.* **2023**, *6*, 172. [CrossRef]
39. Jeong, W.; Shin, H.; Nam, H.; Cho, H.; Heo, J.; Seo, J.; Han, T.H. Nature-Inspired Design of Twisted MXene Heating Wires for Robust Wearable Heating Textiles. *Adv. Funct. Mater.* **2024**, *35*, 2418824. [CrossRef]
40. Jin, S.; Yu, Y.; Xing, J.; Cao, J.; Li, J.; Li, K.; Xiao, H. Versatile synthesis of cellulose film with excellent electrothermal/photothermal dual responsiveness by introducing MXene and small molecule self-assembled nanosphere. *Carbohydr. Polym.* **2024**, *343*, 122441. [CrossRef]
41. Zhao, X.; Peng, L.-M.; Tang, C.-Y.; Pu, J.-H.; Zha, X.-J.; Ke, K.; Bao, R.-Y.; Yang, M.-B.; Yang, W. All-weather-available, continuous steam generation based on the synergistic photo-thermal and electro-thermal conversion by MXene-based aerogels. *Mater. Horiz.* **2019**, *7*, 855–865. [CrossRef]
42. Wang, K.; Chen, C.; Zheng, Q.; Xiong, J.; Liu, H.; Yang, L.; Chen, Y.; Li, H. Multifunctional recycled carbon fiber-$Ti_3C_2T_x$ MXene paper with superior electromagnetic interference shielding and photo/electro-thermal conversion performances. *Carbon* **2022**, *197*, 87–97. [CrossRef]
43. Wang, T.; Gao, S.; Yu, Y.; Chen, Z.; Wang, L.; Zhang, S. Hydrogel Fiber Evaporator with Vertical Channels Integrated with Dual Heat Supply/Insulation Model for Continuous Solar Desalination. *Nano-Micro Lett.* **2026**, *18*, 261. [CrossRef] [PubMed]
44. Zhang, Y.; Zhang, G.; Ma, Z.; Qin, J.; Shen, X. Heterogeneous MXene-based films with graded electrical conductivity towards highly efficient EMI shielding and electrothermal heating. *Nano Res.* **2024**, *17*, 7264–7274. [CrossRef]
45. Xu, C.; Shi, X.; Guo, Y.; Yu, K.; Chen, K. Environmentally responsive dual-compartment microcapsules with full spectrum color-changing performance for anti-counterfeiting applications. *Matter* **2024**, *8*, 101925. [CrossRef]
46. Chen, S.; Liu, D.; Zhang, Y.; Zhang, D.; Chen, Z.; Wu, T.; Feng, X.; Qiu, Z.; Yi, G.; Zhao, Z.; et al. Thermochromic Circularly Polarized Luminescence via Chiral AIEgen-Loaded Microcapsules for Adaptive Camouflage and Security. *Adv. Opt. Mater.* **2025**, *13*, 2500156. [CrossRef]
47. Chen, K.; Chen, J.; Xu, C.; Zhu, H.; Hu, J.; Yu, K. Design and Synthesis of Multi-compartment Microcapsules via Pickering Emulsion Polymerization for Infrared Stealth and Adaptive Camouflage Applications. *Small* **2024**, *21*, 2405543. [CrossRef]
48. Shao, J.; Zhao, X.; Liang, W.; Chen, J.; Shi, Y.; Xu, M.; Zhang, Q.; Chu, L. Electrothermal modulation of MXene-PVDF textiles for advanced infrared thermal shielding. *Nano Res.* **2025**, *19*, 94908291. [CrossRef]
49. Wang, W.; Ma, M.; Song, T.; Chen, J.; Ma, Y.; Yan, C.; Wang, Z.; Ma, D.; Wang, X.; Zhu, X. External Electric Field Enhanced Ti_3C_2 MXene Surface Passivation for Realizing Ultra-Long Cycling Stability. *Small* **2025**, *21*, 2502325. [CrossRef]

Disclaimer/Publisher's Note: The statements, opinions and data contained in all publications are solely those of the individual author(s) and contributor(s) and not of MDPI and/or the editor(s). MDPI and/or the editor(s) disclaim responsibility for any injury to people or property resulting from any ideas, methods, instructions or products referred to in the content.